Observation of vortex dynamics in two-dimensional Josephson-junction arrays

S.G. Lachenmann, T. Doderer, D. Hoffmann, and R. P. Huebener

Physikalisches Institut, Lehrstuhl Experimentalphysik II, Universität Tübingen,
Auf der Morgenstelle 14, D-72076 Tübingen, Germany

P. A. A. Booi and S. P. Benz

National Institute of Standards and Technology, 325 Broadway, Boulder, Colorado 80303

(Received 18 February 1994)

Spatially resolved images of the *dynamic* states of current-biased two-dimensional arrays of Nb/AlO$_x$/Nb Josephson junctions were obtained using low-temperature scanning electron microscopy. The arrays were square or rectangular and the maximum size was 20 junctions × 20 junctions. In overdamped arrays our images at zero or small applied perpendicular magnetic field together with model calculations confirm the nucleation of a vortex at one sample edge (or an antivortex at the opposite edge) and its subsequent motion into the array interior. Vortex annihilation due to vortex-antivortex collision was observed to take place in the middle of the array or at the edge opposite to the nucleation edge. These dynamics and the underlying model considerations are similar to that for Abrikosov vortices in the current-induced resistive state of thin film type-II superconductors. The phenomenon of "row switching" is directly confirmed in images of underdamped arrays. The specific rows experiencing this process change randomly when the same bias point on the current-voltage characteristic is established many times, starting each time from zero current.

I. INTRODUCTION

We report spatially resolved measurements on the *dynamic* behavior in various two-dimensional (2D) Josephson-junction arrays. Arrays of Josephson junctions are interesting for several reasons. They have potential applications as voltage-tunable oscillators or voltage standards. They also represent examples of discrete nonlinear dynamical systems. A detailed understanding of the collective behavior of various array configurations is essential for these applications. Most applications require that all array junctions oscillate in phase. For example, when a Josephson array is used as a voltage-tunable oscillator, the total emitted power to a matched load increases linearly with the number of the phase-locked junctions in the voltage state and the radiation linewidth is inversely proportional to the number in the in-phase state.

Benz and Burroughs reported on coherent emission from two-dimensional arrays.[1,2] In principle, the two-dimensional arrangement of junctions has the advantage that the impedance of the oscillator can be adapted to the load simply by choosing an appropriate ratio of series- and parallel-connected junctions, while keeping the total number of junctions constant. The maximum power coupled from a coherent two-dimensional array to a matched load is proportional to the square of the width (perpendicular to the dc-bias current flow) of the array, giving an additional degree of freedom to increase the available output power. In addition, phase coherence in two-dimensional arrays is expected to be more stable against spreads in the junction critical currents than in series arrays.[3]

Spatially resolved measurements are necessary for understanding the complex oscillatory behavior of 2D arrays. Images of *static* flux configurations in superconducting networks have been shown by several groups.[4-6] In our experiments, we have used the technique of low-temperature scanning electron microscopy (LTSEM) for imaging the *dynamic* behavior. We have investigated overdamped and underdamped square and rectangular arrays of Josephson tunnel junctions. Dealing with overdamped arrays, we address the array dynamics for dc bias currents slightly above the critical current in a regime where no coherent microwave emission was detected. Important information on the collective modes of arrays is obtained from our results, which provide essential input for future optimization of 2D array designs. Furthermore, the phenomenon of row-switching is directly confirmed in images of underdamped arrays.

II. EXPERIMENTAL PROCEDURES

A. Samples

Figure 1 shows the typical array geometry. In 2D arrays, flux quantization has to be taken into account. The total sum of the junction phase differences ϕ around a loop is related to the amount of flux Φ passing through the loop by

$$\sum_{\text{loop}} \phi = -2\pi \frac{\Phi}{\Phi_0} + 2\pi n, \tag{1}$$

where n is an integer and $\Phi_0 = h/2e$ is the flux quantum. The flux Φ can be divided into two parts $\Phi = \Phi^{\text{ext}} + \Phi^{\text{ind}}_{i,j}$, where Φ^{ext} is due to an external magnetic field perpendicular to the array, and $\Phi^{\text{ind}}_{i,j}$ is the self-induced flux
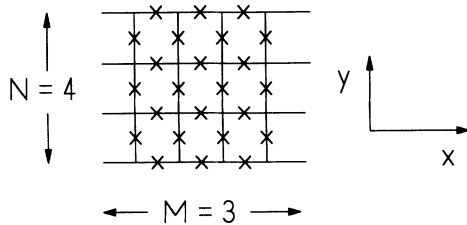
FIG. 1. Sketch of typical array geometry with N columns of M junctions. The arrays consist of rectangular or square networks of superconducting wires with Josephson junctions placed between the line crossings. Each junction is symbolized by a cross (four junction square elementary cell). The notation of the x and y direction is shown. The dc bias current flows in the direction of the x axis. The array voltage drop along the whole array is measured in the same direction.

through the cell (i,j) due to the currents in the array.[7] The frustration f is defined as the applied flux per cell divided by the flux quantum.

The arrays consist of square networks of superconducting microstriplines (Nb and PbInAu) with Josephson junctions placed between the line crossings. The Nb/AlO$_x$/Nb junctions have critical currents on the order of $i_c = 150\,\mu A$. Typically, the 1σ spread in i_c is within 3%.[2] The Josephson coupling energy $E_J = \hbar i_c/2e$ is about $E_J \approx 10^{-20}$ J and is five to six orders of magnitudes larger than the charging energy $E_C = e^2/2C$ (C is the junction capacitance). Hence, we deal with the classical limit, where charging effects can be neglected.[8] The size of the array unit cell is $a \approx 16.7\,\mu m$. Due to this lattice spacing both order parameter and quasiparticle coupling[9] can be ruled out as a coupling mechanism at a temperature of about 5 K. However, the low-frequency interaction of the Josephson junctions due to flux quantization and high-frequency interactions arising from an external load should be taken into account.[10]

We briefly summarize the different types of arrays we have investigated. Further details can be found in [2].

Overdamped arrays with no groundplane (bare arrays). Each of the junctions is externally shunted with an InAu resistor R_s of about 1.5 Ω such that the McCumber parameter is $\beta_{c,j} = 2\pi i_c R_s^2 C/\Phi_0 < 0.7$.[1]

Overdamped arrays coupled to a detector junction. Here, the arrays are coupled by a dc-blocking capacitor to a detector junction. In contrast to the bare arrays described above, a superconducting groundplane is placed on top of the whole circuit at a distance of 0.6 μm. These arrays show coherent emission in the range from 60 to 210 GHz with a maximum power of 0.4 μW.[1,2,11,12]

Underdamped bare arrays. The underdamped arrays are of the same geometry as the bare arrays described above. In contrast to the overdamped arrays, the junction shunt resistors are omitted. The McCumber parameter of the single junctions of the 10 $\times$ 10 array is $\beta_{c,j} \approx 4 \times 10^3$, calculated from the subgap resistance $R_{sg} \approx 150\,\Omega$ and the junction capacitance $C = 0.4\,pF$.[1]

For our spatially resolved investigations we used samples of different sizes $M \times N$: square arrays ($M = N$)

with $M = 6,10,20$ and rectangular arrays with $M = 20$ and $N = 10$.

B. Electron beam imaging

LTSEM enables the spatially resolved investigation of superconducting devices and circuits during their operation at liquid-helium temperatures. The basic principles are reported in Ref. 13. The essential points are the following: the sample film (on the top side of the substrate) is irradiated directly with the electron beam. The bottom side of the substrate is in contact with the liquid-helium bath, thus ensuring effective sample cooling. The electron beam focused at the coordinates (x_0,y_0) on the sample surface acts as a local heat source. The lateral dimension of the thermally perturbed area near (x_0,y_0) determines the spatial resolution of our imaging procedure. This resolution is estimated to be about 3 μm for our samples. Typical values for the beam voltage and current are 25 kV and 100 pA, respectively, yielding a local temperature increment of about 1 K.

The difference of the time scales of the array dynamics and of the scanning procedure is important. The junction oscillation period is on the order of 10 ps, whereas the decay time of the beam's thermal perturbation is about 100 ns.[13] During scanning, the electron beam typically stays 3 ms at each position. The measured sample response to the beam irradiation represents time-averaged information on the time scale of the Josephson dynamics.

The sample is well shielded from dc and ac magnetic fields by means of μ-metal shielding at both room and liquid-helium temperature. During our measurements, the electron beam is scanned across the current-biased array. The beam is chopped at a frequency of 20 kHz and the change in array voltage $\Delta V(x_0,y_0)$ induced by the beam, is phase sensitively recorded using a lock-in technique. Near the beam focus, the junctions are heated from about 5 to 6 K, which reduces the critical current i_c of a junction by 20%. In these experiments, the local heating induces a voltage signal $\Delta V(x_0,y_0)$ of about 10 μV or less.

III. RESULTS AND DISCUSSION

In this section we present the main results of our spatially resolved investigations of the two-dimensional Josephson junction arrays.

A. Overdamped arrays

Figure 2 shows the voltage signal $\Delta V(x_0,y_0)$ for the overdamped 10×10 array without ground plane. The array is current biased at 1.5 mA and a corresponding voltage of 1 mV. The array critical current is $I_c \approx 1$ mA. In Fig. 2(a), a positive (negative) signal $\Delta V(x_0,y_0)$ is indicated by the bright (dark) areas, whereas the zero signal level is shown by the gray area surrounding the array. In Fig. 2(b), a vertical line scan along row No. 3 of Fig. 2(a) is shown. The most pronounced features are large positive and negative voltage signals at the upper and
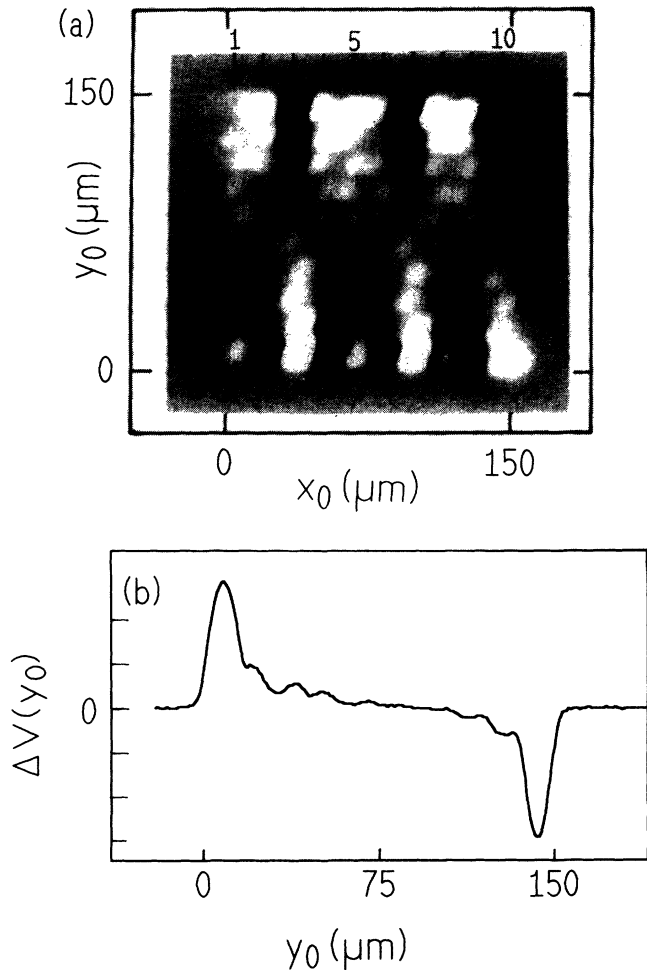
(a)

(b)

FIG. 2. (a) Gray value representation of the voltage image $\Delta V(x_0, y_0)$ for the 10×10 overdamped array without ground plane at $T \approx 5$ K. The externally applied magnetic field is zero. The array is current biased at 1.5 mA and a voltage of 1 mV. The array critical current is $I_c \approx 1$ mA. The dc bias current flows horizontally through the array. The array boundaries lie between 0 and 150 μm in both directions. A positive (negative) electron-beam-induced signal $\Delta V(x_0, y_0)$ is indicated by the bright (dark) areas, whereas $\Delta V(x_0, y_0) \approx 0$ is shown by the areas surrounding the array. The individual rows of junctions are indicated by the small arrows numbered 1–10 from left to right. (b) Voltage signal profile $\Delta V(y_0)$ (in arbitrary units) along a linear vertical scan across row No. 3 shown in part (a). The array is located between $y_0 = 0$ and 150 μm.

lower edges of the array. Positive and negative signal peaks appear at the locations of the junctions.

Figure 3 shows the voltage signal of a single row of the 20 × 20 array without ground plane. The line scan is perpendicular to the bias current direction. The bias current is 1.2 mA, and the corresponding array voltage is 1 mV. This array has a critical current of $I_c \approx 1.1$ mA. Again, large positive and negative voltage signals appear near the two opposite edges of the array. Figures 2 and 3 are characteristic examples for the voltage images, which we observed in different sized arrays without ground plane
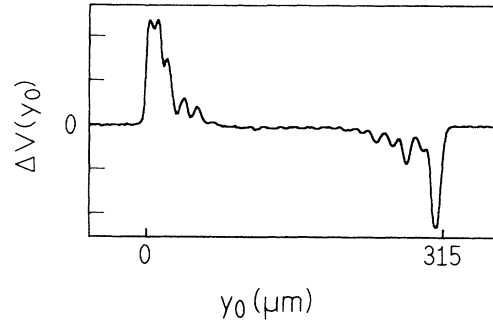

FIG. 3. Voltage signal profile $\Delta V(y_0)$ (in arbitrary units) of a vertical scan across a row of junctions in the 20×20 array. The array is located between $y_0 = 0$ and 315 μm. $T \approx 5$ K. The externally applied magnetic field is zero.

either with a bias current slightly above I_c without external magnetic fields or with a transverse applied magnetic field less than $f \approx 4$.

The voltage along the array in the direction of the applied current is due to junction phase slips. In the simplest case, the current flows only along the lines of the network oriented in the x direction, and the lines in the y direction remain free of current. In this case phase slips occur only in the junctions belonging to the lines in the x direction, and phase coherence between points with the same x coordinate is preserved by means of the superconducting wires (or connections) in the y direction. Deviations from the in-phase state may occur in the form of vortex motion across the array, where vortices are driven by the Lorentz-force perpendicular to the bias current. A junction phase slips relative to neighboring junctions when a vortex moves across. Vortices can be induced in an array with an applied magnetic field, or from self-induced fields. There is a close analogy between the vortex dynamics in superconducting thin films and 2D Josephson arrays.[10] From this analogy we expect that for the zero voltage state of the array, the supercurrent flows mainly along the sample edges, establishing the Meissner effect in the inner regions of the sample. In the resistive state we expect the nucleation of magnetic flux quanta at the sample edge and their subsequent motion across the sample perpendicular to the current direction. The electromagnetic radius of the vortex is given by the magnetic penetration depth $\lambda_\perp = \Phi_0/(2\pi\mu_0 i_c)$, where μ_0 is the permeability of free space.[10] For the arrays we have studied $\lambda_\perp$ is about 10 μm, which is about 0.6a. The dynamics of the nucleation and motion of vortices in 2D Josephson arrays can be treated in close analogy to the situation of Abrikosov vortices in superconducting thin films.[14–16] In particular, the driving force acting on the vortex is found from the spatial dependence of the Gibbs energy $U(y)$ of a single vortex. Neglecting self-field effects,[7] $U(y)$ contains five contributions for a single vortex in a 2D array:[17–19] the vortex energy in zero magnetic field $U_0(y)$, the energy $U_f(y)$ and $U_i(y)$ due to the vortex interaction with an external magnetic field and an applied transport current, respectively, and the core energy $U_c(y)$. Further, in 2D-Josephson junction arrays the periodic two-dimensional potential energy U_{pot} also

must be taken into account.[18,19] Noting that the penetration depth $\lambda_\perp$ is about the cell size, the energy barrier between adjacent unit cells is $E_B \approx 0.3 E_J$.[7] Hence, we have

$$\tilde{U}(\tilde{y}) = \tilde{U}_0(\tilde{y}) + \tilde{U}_f(\tilde{y}) + \tilde{U}_i(\tilde{y}) + \tilde{U}_c(\tilde{y}) + \tilde{U}_{\text{pot}}(\tilde{y}) \qquad (2)$$

with

$$\tilde{U}_0(\tilde{y}) = \pi \ln \left[\frac{2\tilde{W}}{\pi} \cos \left(\frac{\pi \tilde{y}}{\tilde{W}} \right) \right], \qquad (3)$$

$$\tilde{U}_f(\tilde{y}) = \frac{-\pi^2 \tilde{W}^2}{2} f \left[1 - 4 \left(\frac{\tilde{y}}{\tilde{W}} \right)^2 \right], \qquad (4)$$

$$\tilde{U}_i(\tilde{y}) = -2\pi \frac{I}{I_c} \left(\tilde{y} + \frac{1}{2}\tilde{W} \right), \qquad (5)$$

$$\tilde{U}_c(\tilde{y}) = \frac{\pi^2}{2}, \qquad (6)$$

$$\tilde{U}_{\text{pot}}(\tilde{y}) = -\frac{1}{2} 0.3 \cos(2\pi \tilde{y}). \qquad (7)$$

$\tilde{U} = U/E_J$ denotes the normalized energy, $\tilde{y} = y/a$ and $\tilde{W} = W/a$ the normalized y coordinate and width, respectively. The $\tilde{y}$ coordinate is measured from the middle of the array. Since E_J, being proportional to the junction's critical current i_c, depends on temperature, all energies are temperature dependent. The presence of a bias current yields a significant asymmetry of the force felt by a vortex entering or leaving the array.

$\tilde{U}_0(\tilde{y})$ shows a logarithmic singularity at the two array boundaries $\tilde{y} = \pm \tilde{W}/2$, where vortex nucleation and annihilation takes place. Both, nucleation and annihilation of a vortex are beyond the scope of our model, and the array boundaries have to be considered separately. In the simplest case one can use a proper truncation approximation. To omit this singularity, we calculated $\tilde{U}(\tilde{y})$ from $\tilde{y} = -\tilde{W}/2 + \tilde{\lambda}_\perp/2$ to $\tilde{y} = \tilde{W}/2 - \tilde{\lambda}_\perp/2$, with $\tilde{\lambda}_\perp = \lambda_\perp/a$. Furthermore, for simplicity, a uniform bias current distribution is assumed for describing the vortex motion inside the array.

Figure 4 shows $\tilde{U}(\tilde{y})$ calculated from Eqs. (2)–(7) for the transport current of $1.5 I_c$ in the overdamped bare 10×10 array. The force acting on a single vortex is $-\partial U/\partial y$. For dynamic equilibrium this force is balanced by the damping force ηv, so

$$-\frac{\partial U}{\partial y} - \eta v = 0. \qquad (8)$$

The damping coefficient is $\eta = \Phi_0^2/(2Sr)$, where S is the area of the unit cell, and r is the shunt resistance of each junction.[21] With $S \approx (16.7\,\mu\text{m})^2$ and $r \approx 1.5\,\Omega$, we obtain $\eta \approx 5*10^{-21}$ kg/s. In the overdamped arrays, the inertia term in the force equation (8) can be neglected. In Fig. 5 we present the vortex velocity $v(\tilde{y})$ for the same parameters as in Fig. 4. Near the point of vortex
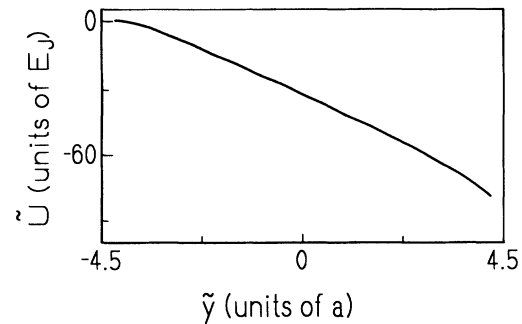

FIG. 4. The energy $\tilde{U}(\tilde{y})$ of a single vortex versus the $\tilde{y}$ coordinate. $\tilde{U}(\tilde{y})$ is calculated from Eqs. (2)–(7) neglecting self-induced fields for the following parameters: width of the array is nine unit cells, corresponding to 10 junctions in each row. The bias current is $I = 1.5 I_c$, where I_c is the array critical current. The external magnetic field is zero ($f = 0$). The energy is measured in units of the Josephson coupling energy E_J. The width W of the array along the y-axis is given in units of elementary cells a. The $\tilde{y}$ coordinate is measured from the middle of the array. The calculation is truncated at $\tilde{\lambda}_\perp/2$ from both edges of the array.

entry and exit at $\tilde{y} = -4.5$ and $\tilde{y} = +4.5$, respectively, the velocity $v(\tilde{y})$ shows a rapid increase with increasing $\tilde{y}$ coordinate. This can be qualitatively understood in terms of the attractive interaction between the vortex and its image vortex. At the point of vortex entry, the additional force is acting in the opposite direction as the driving Lorentz force. At the point of vortex exit it is acting in the same direction as the Lorentz force.[14]

The electron beam irradiation causes a local temperature increase and affects the vortex velocity $v(y)$ in the following way. The critical current of the irradiated junction is decreased by the amount $\Delta i_c/i_c \approx 0.2$. Therefore the Josephson coupling energy of the irradiated junction is reduced. Because all five parts of the single vortex energy in Eq. (2) are proportional to the coupling energy, the whole energy and also the velocity profile of the vortex along the array (perpendicular to the bias current) is changed. For a first approximation, we consider the velocity function $v(y)$ for two different array temperatures T_1 and T_2, where T_1 is the temperature in the area heated by the electron beam, and T_2 is the temperature in the remaining undisturbed region ($T_1 > T_2$). For T_1 and T_2 we calculate the two vortex velocity profiles
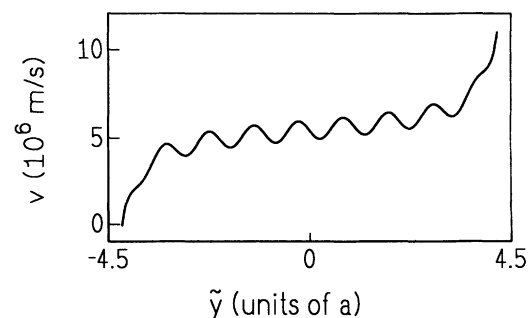

FIG. 5. Velocity v of a single vortex vs the $\tilde{y}$ coordinate for the same parameters as in Fig. 4. The calculation is truncated at $\tilde{\lambda}_\perp/2$ from both edges of the array.

$v_1(y)$ and $v_2(y)$, expressing the two different tempera-
tures in terms of different values of the critical current
of the array. A typical curve for the velocity difference
$\Delta v(\tilde{y}) = v_1(\tilde{y}) - v_2(\tilde{y})$ is shown in Fig. 6(a), indicating
that Δv strongly depends on the actual vortex position in
the array. We expect that the beam-induced local tem-
perature increment of the junction near the coordinate
y_0 causes a local vortex velocity change depending on y_0
similarly to the calculated difference Δv shown in Fig.
6(a). The beam-induced velocity change calculated from
the curve in Fig. 6(a) for the location of the different
junctions is shown in Fig. 6(b). Again, the two outer
junctions at $y_0 = 0$ and $y_0 = 150\,\mu$m have been omitted
due to our truncation approximation. The curve $\Delta v(\tilde{y})$
shows point symmetry with respect to the coordinate ori-
gin $\Delta v = 0$ and $\tilde{y} = 0$. This is understood, if we look at
the symmetry properties of Eqs. (3)–(7) with respect to
a sign reversal of $\tilde{y}$. Again, the large positive and nega-
tive values of Δv near the points of vortex entry and exit,
respectively, can be related to the attractive interaction
between the vortex and its image vortex near the outer
edges of the array. We expect that the velocity difference
$\Delta v(y_0)$ is proportional to the voltage signal $\Delta V(y_0)$. The
voltage signal $\Delta V(y_0)$ expected from the velocity profile
$\Delta v(y_0)$ in Fig. 6 agrees qualitatively with the line scans

FIG. 7. Schematic display of the vortex motion found by
inspection of Fig. 2(a). The dc bias current flows horizontally
through the array. $\oplus$ and $\ominus$ denote the vorticity of a vortex
and an antivortex, respectively. The rows of junctions are
numbered as in Fig. 2(a).

presented in Fig. 2 and 3.

Three cases are possible for the motion of current in-
duced vortices driven by the Lorentz force across the
sample in zero applied magnetic field: (1) simultaneous
nucleation of a vortex and an antivortex at the two oppo-
site edges, respectively, both moving towards the center
where they annihilate; (2) nucleation of a single vortex
at one sample edge, moving subsequently to the opposite
edge; (3) the inverse process of case (2) for an antivortex.
All three possibilities were observed in the same sample
as seen in Fig. 2. Figure 7 shows a sketch of the vortex
dynamics for the situation in our experiment presented
in Fig. 2 . Case (1) is seen in rows 1 and 5; case (2) in
rows 2, 4, 6, 8, and 9; case (3) in rows 3, 7, and 10. It
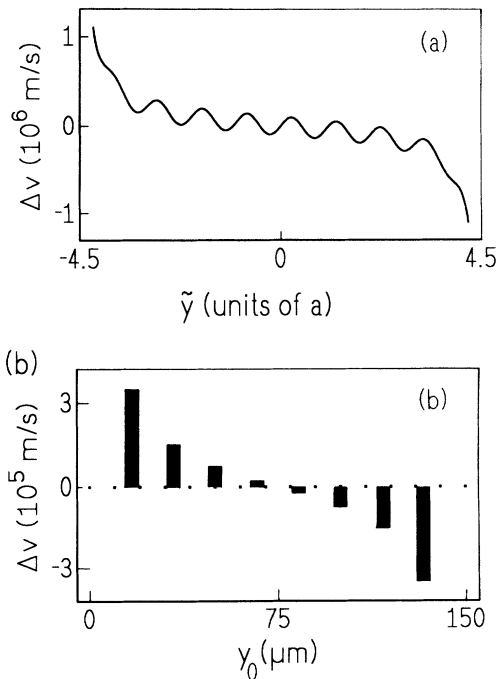is interesting, that along the current direction there is a

FIG. 6. (a) The difference $\Delta v(\tilde{y}) = v_1(\tilde{y}) - v_2(\tilde{y})$ for two
different temperatures. Critical currents of $i_{c,1} = 120$ and 150
μA were used to calculate $v_1(\tilde{y})$ and $v_2(\tilde{y})$, respectively. The
different critical currents i_c correspond to two different tem-
peratures. In both cases, the bias current is $I = 1.5I_c$, where
I_c is the array critical current corresponding to $i_{c,2}$. (b) The
electron-beam-induced vortex velocity change as a function of
y_0. The eight peaks correspond to the inner junctions in the
array where the heating results in a vortex velocity change
according to (a). The signal peaks of the two junctions at the
boundaries ($y_0 = 0$ and 150 μm) are omitted because of our
truncation approximation. The velocity difference $\Delta v(y_0)$ is
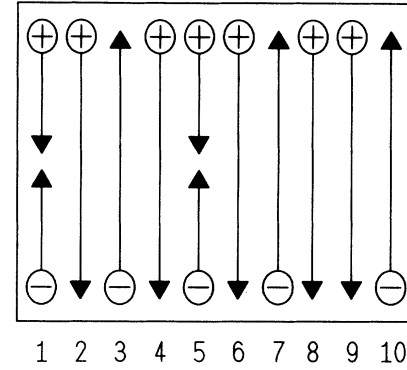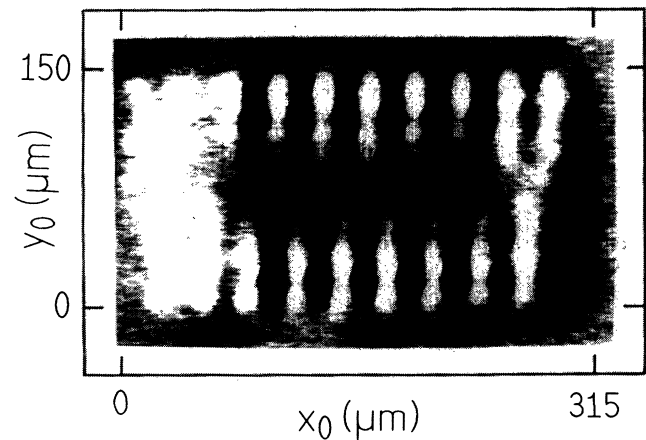proportional to the voltage signal $\Delta V(y_0)$.

FIG. 8. Gray value representation of the voltage image
$\Delta V(x_0, y_0)$ for the 20×10 array with groundplane at $T \approx 5$
K. The array is current biased at 1.25 mA and a correspond-
ing voltage of 3 mV. The array critical current is $I_c \approx 750\,\mu$A.
The dc bias current flows horizontally through the array. The
array boundaries lie between 0 and 150 μm in y direction and
between 0 and 315 μm in the x direction. A positive (nega-
tive) electron-beam-induced signal $\Delta V(x_0, y_0)$ is indicated by
the bright (dark) areas, whereas $\Delta V(x_0, y_0) \approx 0$ is shown by
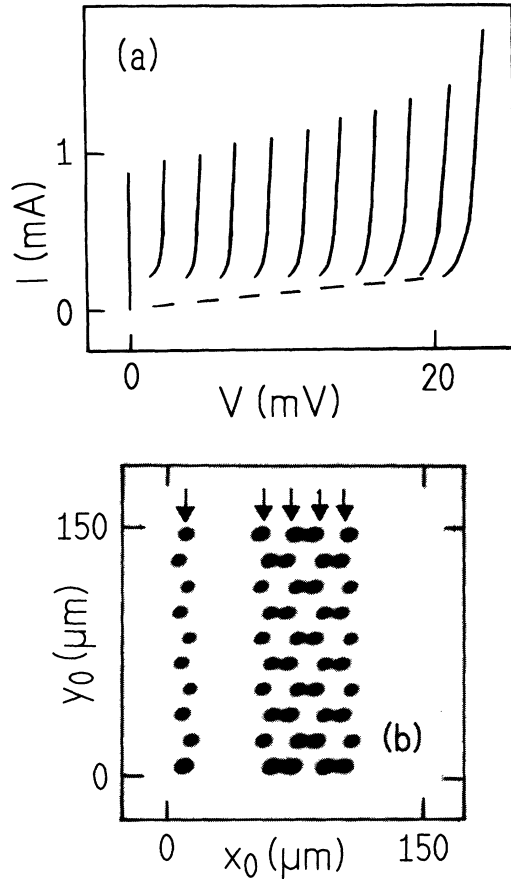the gray value of the areas surrounding the array.

FIG. 9. (a) Current-voltage characteristic of an under-damped 10×10 array without groundplane at $T \approx 5$ K. The externally applied magnetic field is zero. I denotes the applied dc-bias current and V the dc-voltage across the array. (b) Gray value representation of the voltage image $\Delta V(x_0,y_0)$ for the same array at $T \approx 5$ K. The externally applied magnetic field is zero. The array is current biased at 0.5 mA on the fifth step. The corresponding voltage is 11 mV. The array critical current is $I_c \approx 0.8$ mA. The dc-bias current flows horizontally through the array. The array boundaries lie between 0 and 150 μm in both directions. A negative electron beam induced signal $\Delta V(x_0,y_0)$ is indicated by the dark areas, whereas $\Delta V(x_0,y_0) \approx 0$ is shown by the gray value of the areas surrounding the array. The five rows of junctions being in the voltage state are indicated by small arrows.

B. Underdamped arrays: Direct observation of row switching

The current-voltage characteristic (IVC) of the hysteretic 10×10 bare array is shown in Fig. 9(a). It shows 10 pronounced steps, equally spaced along the voltage axis. The distance between the steps is the gap voltage $2\Delta/e$, where Δ is the energy gap of Niobium, and e is the elementary charge. Figure 9(b) shows an example of an LTSEM voltage image when the array is current-biased on the fifth step. The dark spots correspond to the junctions, which are in a finite voltage state. Biasing the array on the nth step, we always observed that the junctions of n rows are in the voltage state. This phenomenon has been discussed as row switching,[20-22] which was only indirectly deduced up to now. The McCumber-Parameter of the single junctions in this array is $\beta_c \approx 4 \times 10^3$. For such small damping, it is expected that the vortex lattice has no region of dynamic stability.[22] As soon as the vortices are depinned by the bias current they reach a high kinetic energy and induce a switch to a finite voltage state of all junctions in their path. We always found by direct imaging that only entire rows of junctions are switched into the voltage state. Establishing the same bias point on the IVC many times, starting again from zero current, we have found that only the total number of rows undergoing the switching process remained fixed. On the other hand, the individual rows "selected" for this process changed randomly.

IV. CONCLUSIONS

We observed the dynamics of field-induced vortices in two-dimensional Josephson-junction arrays in a region of low bias current slightly above the critical current. In this region no coherent microwave radiation emission was detected from the samples having an on-chip microwave radiation detector. Deviations from the in-phase oscillation of the junctions may therefore be attributed to vortex motion in the array.

tendency to alternate between case (2) and (3). Such alternation is expected from the repulsion between vortices of the same vorticity.

In Figure 8 we show an imaging result obtained with a 20×10 array with a ground plane. As for the arrays without ground plane, we observe the same dynamics of the current-induced vortices for bias currents slightly above I_c, where no coherent microwave emission could be detected with the on-chip detector junction coupled to the array. In Fig. 8 cases (2) and (3) are alternating with each other from row to row in the main part of the array.

[1]S. P. Benz and C. J. Burroughs, Appl. Phys. Lett. **58**, 2162 (1991).

[2]S. P. Benz and C. J. Burroughs, Supercond. Sci. Technol. **4**, 561 (1991).

[3]M. Octavio, C. B. Whan, and C. J. Lobb, Appl. Phys. Lett. **60**, 766 (1992).

[4]L. N. Vu, M. S. Wistrom, and D. J. Van Harlingen, Appl. Phys. Lett. **63**, 1693 (1993).

[5]K. Runge and B. Pannetier, Europhys. Lett. **24**, 737 (1993).

[6]H. D. Hallen, R. Seshadri, A. M. Chang, R. E. Miller, L. N. Pfeiffer, K. W. West, C. A. Murray, and H. F. Hess, Phys. Rev. Lett. **71**, 3007 (1993).

[7]J. R. Phillips, H. S. J. van der Zant, J. White, and T. P. Orlando, Phys. Rev. B **47**, 5219 (1993).

[8]H. S. J. van der Zant, F. C. Fritschy, T. P. Orlando, and J. E. Mooij, Phys. Rev. B **47**, 295 (1993).

[9]A. K. Jain, K. K. Likharev, J. E. Lukens, and J. E. Sauvageau, Phys. Rep. **109**, 309 (1984).

[10]K. K. Likharev, *Dynamics of Josephson Junctions and Circuits* (Gordon and Breach, New York, 1986).

[11]T. Doderer, D. Hoffmann, R. P. Huebener, N. Kirchmann, C. A. Krulle, S. Lachenmann, D. Quenter, J. Schmidt, S. Stehle, J. Niemeyer, R. Pöpel, S. P. Benz, and P. A. A. Booi, IEEE Trans. Appl. Supercond. **3**, 2724 (1993).

[12]P. A. A. Booi, S. P. Benz, T. Doderer, D. Hoffmann, J. Schmidt, S. Lachenmann, and R. P. Huebener, IEEE Trans. Appl. Supercond. **3**, 2493 (1993).

[13]R. P. Huebener, in *Advances in Electronics and Electron Physics*, edited by P. W. Hawkes (Academic, New York, 1988), Vol. **70**, p. 1.

[14]J. R. Clem, R. P. Huebener, and R. P. Gallus, J. Low Temp. Phys. **12**, 449 (1973).

[15]L. G. Aslamazov and A. I. Larkin, Zh. Eksp. Teor. Fiz. **68**, 766 (1975) [Sov. Phys. JETP **41**, 381 (1975)].

[16]W. Buck, J. Parisi, and B. Mühlemeier, J. Low Temp. Phys. **55**, 51 (1984).

[17]H. S. J. van der Zant, H. A. Rijken, and J. E. Mooij, J. Low Temp. Phys. **79**, 289 (1990).

[18]C. J. Lobb, D. W. Abraham, and M. Tinkham, Phys. Rev. B **27**, 150 (1983).

[19]M. S. Rzchowski, S. P. Benz, M. Tinkham, and C. J. Lobb, Phys. Rev. B **42**, 2041 (1990).

[20]H. S. J. van der Zant, C. J. Muller, L. J. Geerlings, C. J. P. M. Harmans, and J. E. Mooij, Phys. Rev. B **38**, 5154 (1988).

[21]U. Geigenmüller, C. J. Lobb, and C. B. Whan, Phys. Rev. B **47**, 348 (1993).

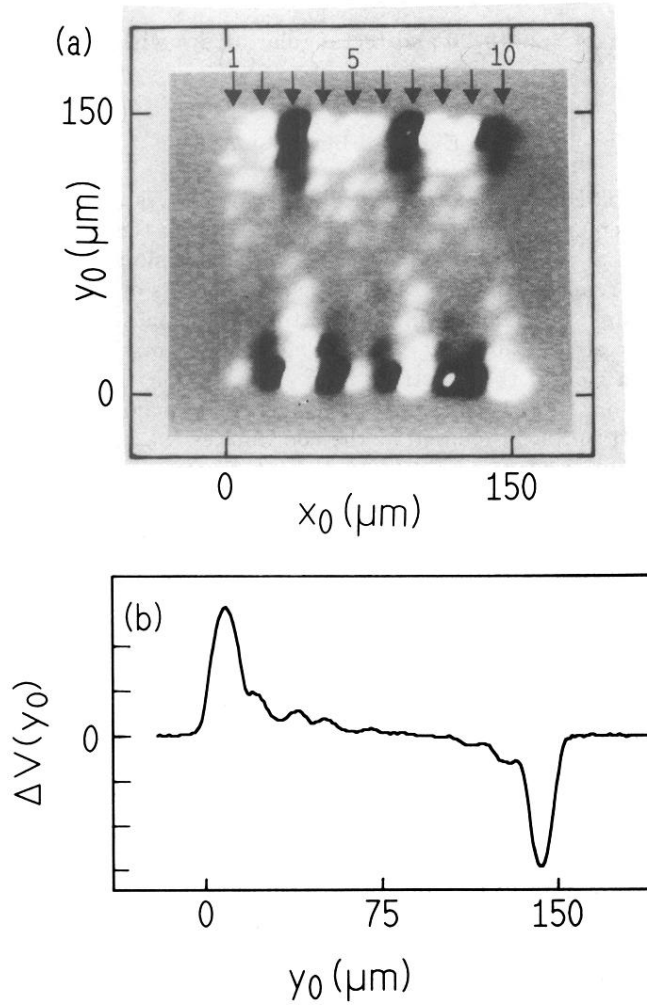[22]W. Yu, K. H. Lee, and D. Stroud, Phys. Rev. B **47**, 5906 (1993).

FIG. 2. (a) Gray value representation of the voltage image $\Delta V(x_0, y_0)$ for the 10×10 overdamped array without ground plane at $T \approx 5$ K. The externally applied magnetic field is zero. The array is current biased at 1.5 mA and a voltage of 1 mV. The array critical current is $I_c \approx 1$ mA. The dc bias current flows horizontally through the array. The array boundaries lie between 0 and 150 μm in both directions. A positive (negative) electron-beam-induced signal $\Delta V(x_0, y_0)$ is indicated by the bright (dark) areas, whereas $\Delta V(x_0, y_0) \approx 0$ is shown by the areas surrounding the array. The individual rows of junctions are indicated by the small arrows numbered 1–10 from left to right. (b) Voltage signal profile $\Delta V(y_0)$ (in arbitrary units) along a linear vertical scan across row No. 3 shown in part (a). The array is located between $y_0 = 0$ and 150 μm.
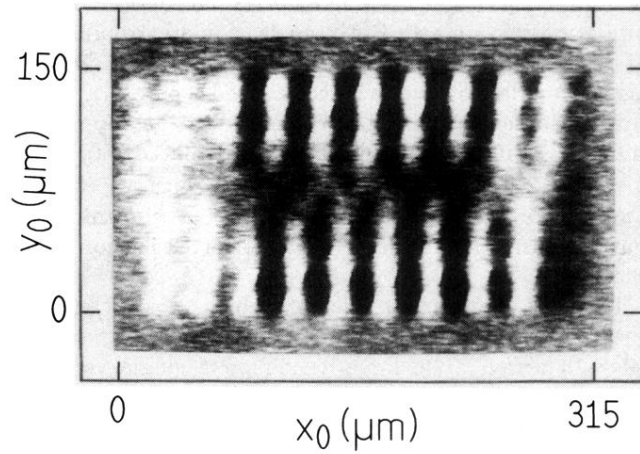
FIG. 8. Gray value representation of the voltage image $\Delta V(x_0, y_0)$ for the 20×10 array with groundplane at $T \approx 5$ K. The array is current biased at 1.25 mA and a corresponding voltage of 3 mV. The array critical current is $I_c \approx 750\ \mu$A. The dc bias current flows horizontally through the array. The array boundaries lie between 0 and 150 μm in y direction and between 0 and 315 μm in the x direction. A positive (negative) electron-beam-induced signal $\Delta V(x_0, y_0)$ is indicated by the bright (dark) areas, whereas $\Delta V(x_0, y_0) \approx 0$ is shown by the gray value of the areas surrounding the array.
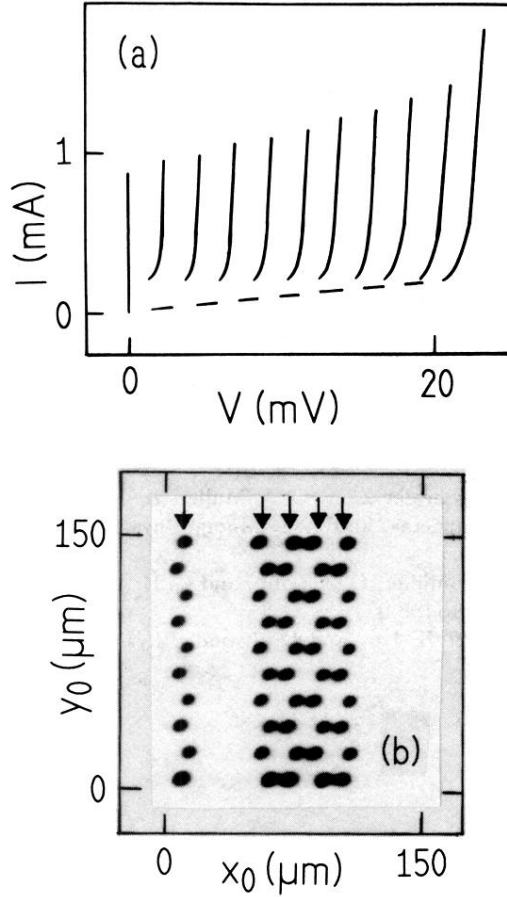
FIG. 9. (a) Current-voltage characteristic of an under-damped 10×10 array without groundplane at $T \approx 5$ K. The externally applied magnetic field is zero. I denotes the applied dc-bias current and V the dc-voltage across the array. (b) Gray value representation of the voltage image $\Delta V(x_0, y_0)$ for the same array at $T \approx 5$ K. The externally applied magnetic field is zero. The array is current biased at 0.5 mA on the fifth step. The corresponding voltage is 11 mV. The array critical current is $I_c \approx 0.8$ mA. The dc-bias current flows horizontally through the array. The array boundaries lie between 0 and 150 μm in both directions. A negative electron beam induced signal $\Delta V(x_0, y_0)$ is indicated by the dark areas, whereas $\Delta V(x_0, y_0) \approx 0$ is shown by the gray value of the areas surrounding the array. The five rows of junctions being in the voltage state are indicated by small arrows.